# Portable Thomson scattering system for temporally resolved plasma measurements under low density conditions

N. Yamamoto 💿 ; A. P. Yalin 💌 📵



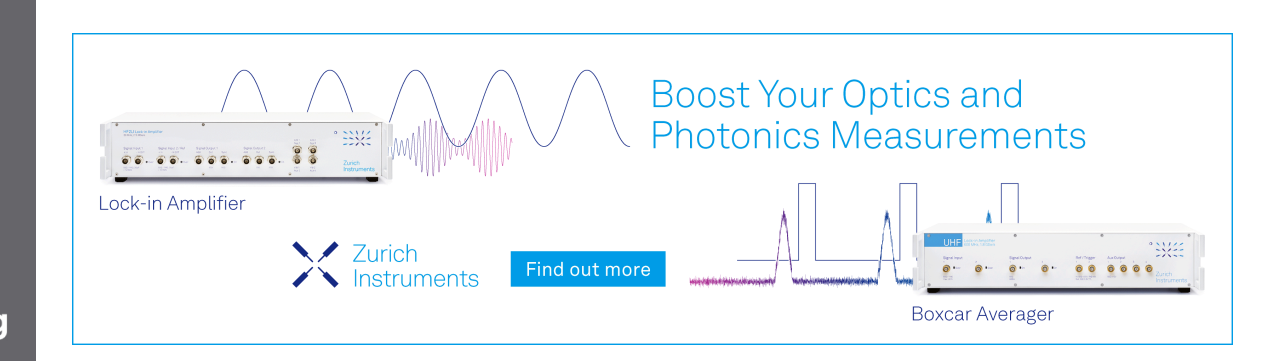
Rev. Sci. Instrum. 95, 033502 (2024)

https://doi.org/10.1063/5.0180534





CrossMark





16 March 2024 16:55:21

# Portable Thomson scattering system for temporally resolved plasma measurements under low density conditions

Cite as: Rev. Sci. Instrum. 95, 033502 (2024); doi: 10.1063/5.0180534 Submitted: 10 October 2023 • Accepted: 12 February 2024 • Published Online: 7 March 2024









N. Yamamoto<sup>1</sup> and A. P. Yalin<sup>2,a)</sup>



## **AFFILIATIONS**

- Department of Interdisciplinary Engineering Sciences, Kyushu University, Kasuga 816-8580, Japan
- Department of Mechanical Engineering, Colorado State University, Fort Collins, Colorado 80524, USA
- a) Author to whom correspondence should be addressed: azer.yalin@colostate.edu

#### **ABSTRACT**

We present the development of a portable Thomson scattering diagnostic system allowing simultaneous spatially and temporally resolved plasma property measurements for low density plasmas. The setup uses a compact pulsed Nd:YAG laser (532 nm) as the light source with suppression by two volume Bragg grating notch filters and dispersion with a single-stage spectrometer before measurement with an intensified camera. A key issue is the detailed light collection and how it impacts the sensitivity and elastic light suppression, for which we have investigated two optical configurations, one based on a 7 × 1 linear fiber bundle and the other based on a slit spatial-filter. We find that the configuration with the slit spatial-filter provides a higher sensitivity by a factor of ~2 along with more uniform spatial response. We have developed a custom pulsed-plasma setup with a modulation at 20 kHz, representative of the Hall thruster breathing mode oscillation, to show the possibility of temporally resolved measurements for electric propulsion applications. We have successfully recorded the variations in electron number density and temperature with sub-mm spatial resolution and capturing ten temporal points over the 50  $\mu$ s modulation period. The detection limit of electron density (with the spatial-filter configuration) is  $\sim 1.6 \times 10^{17}$  m<sup>-3</sup>, which is  $\sim 1/10$  of the plasma density in the acceleration channel of Hall thrusters.

Published under an exclusive license by AIP Publishing. https://doi.org/10.1063/5.0180534

#### I. INTRODUCTION

Diagnostics by laser Thomson scattering (LTS)<sup>1-3</sup> provide a powerful tool for understanding the physics of complex plasma behavior and for developing plasma sources, including for electric propulsion (EP) applications. 4-6 LTS can provide detailed information on plasma properties (typically electron density and temperature) without perturbing the target plasma, so many studies have been conducted using this technique for fusion plasmas, extreme ultraviolet lithography light sources,7 and industrial plasma

Because LTS is an elastic light scattering method, the signal spectrum is close to the laser wavelength such that the suppression of laser (Rayleigh) and elastically scattered stray background light (from windows, electrodes, etc.) is a major experimental challenge. Conventional LTS implementations require a relatively large probe laser source as well as a complex spectrometer, such as a triple grating spectrometer9 (where the first two stages are used in a subtractive mode) or even a six grating spectrometer, <sup>10</sup> for the rejection of the strong stray light and Rayleigh scattering light. The technique also tends to require quite laborious alignment work to improve the signal-to-noise ratio (S:N). A further challenge to widespread adoption is the very low (wavelength-independent) Thomson scattering cross section, which manifests as very low signal levels. For cases where the plasma density is less than ~10<sup>18</sup> m<sup>-3</sup>, it typically takes several tens of minutes to measure plasma properties under one condition. This issue is particularly problematic for cases where it is desired to gather temporally resolved Thomson scattering data, for example as would be very helpful to understand oscillations in Hall thrusters that are widely used for EP. A prevalent oscillation in Hall thrusters is the breathing mode oscillation, which has been widely studied both numerically 11-14 and experimentally, 15-20 and despite its identification and early characterization nearly 50 years ago, 15 it remains an active area of research. This oscillation is described

by strong, coherent, low-frequency fluctuations in the discharge current, typically between  ${\sim}10$  and 30 kHz during which electron densities can fluctuate from  ${\sim}10^{17}$  to  $10^{18}$  m $^{-3}.^{21}$  In addition to being of theoretical interest, the breathing mode oscillation can lead to modal transitions in thruster operation, which critically impact the in-space performance of the thruster.  $^{22}$  Indeed, the previous time-resolved Thomson scattering measurement has been conducted in much denser plasmas.  $^{7,10,23}$ 

The focus of the present article is to develop a relatively portable temporally resolved Thomson scattering measurement system to enable measurements at low plasma densities as is of interest, for example, in EP applications and which may also be applicable for studies of sources used in the semiconductor industry. Extending to temporally resolved is challenging since measurements essentially need to be performed over another dimension (we use ten temporal bins) such that further improvements in S:N are required. Our article builds upon related groundbreaking work from Vincent et al.24 and Bak et al.,25 who have shown that volume Bragg grating (VBG) notch filter(s) can be used for light suppression in LTS in place of the more conventionally used triple grating spectrometers. (Note that in addition to cost and complexity of operation, these instruments typically are also quite large and massive, for example, dimensions of ~800 × 800 × 200 mm<sup>3</sup> and weight of ~30 kg for the SPEX-1877.) Herein, we also use VBG notch filters for spectral suppression, but relative to past articles studying low density plasmas, we develop a system with an improved S:N (influenced by both sensitivity and suppression) based on the incorporation of a one-dimensional spatial-filter in the imaging system. The resulting configuration allows, for the first time, simultaneous spatial and temporal resolution in low-density oscillating plasmas. Furthermore, the system employs relatively compact components and thus can also be portable between measurement locations and laboratories. The setup is described in detail in Sec. II. The measurement results, including detailed optical characterizations as well as spatially and temporally resolved plasma properties from a pulsed plasma, are presented in Sec. III, while conclusions are given in Sec. IV.

# II. EXPERIMENTAL SETUP

Figure 1 shows the setup of the portable laser Thomson scattering measurement system. We use a compact second-harmonic Nd:YAG laser (Quantel Q-Smart 100) as the probe laser. The laser head is about 90 × 90 × 300 mm³, and the power supply is ~400 × 200 × 350 mm³. Several high reflectivity mirrors are used in order to adjust the polarization plane, which is set perpendicular to the plane of the scattering. The laser wavelength is 532 nm, and the pulse energy is fixed at 50 mJ with a pulse repetition rate of 20 Hz and a pulse duration of 8 ns. The laser light is weakly focused to the measurement region with a 500 mm focal length lens. To reduce the scattering of stray light, the cell is instrumented with Brewster windows on either end as well as a series of annular baffles along the laser axis. The probe laser and delivery optics are also enclosed within cardboard tubes with a view dump positioned in the opposite direction of the collection optics.

The collected light, including Thomson scattering, is dispersed using a compact 150 mm focal length spectrometer with a grating

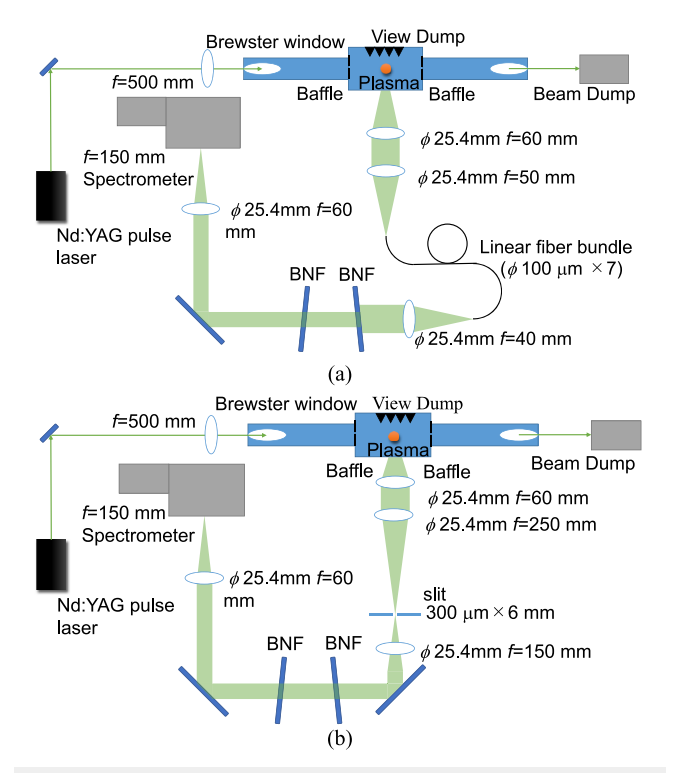


**FIG. 1.** Optical system for the portable Thomson scattering measurement. (a) Using a  $7 \times 1$  linear fiber bundle and (b) using a slit spatial-filter.

of 1800 grooves per mm (Princeton Instruments, model SP-2156,  $178 \times 178 \times 165 \text{ mm}^3$ ). The compact spectrometer allows the system to be far more potable as compared to our previous triple grating spectrometer (SPEX-1877). The calculated dispersion of the spectrometer setup is 2.37 nm/mm. Wavelength calibration was performed with two methods, the first based on line emission from the studied argon plasma (see below) and the second based on the known spectral characteristics of rotational Raman scattering from nitrogen (e.g., Friss and Yalin<sup>26</sup>). The entrance slit of the spectrometer is set as 150  $\mu$ m. The instrumental function of the spectrometer in this study is 0.15 nm. For the suppression of the stray light and Rayleigh scattering light, two VBG notch filters are used instead of a triple grating spectrometer (with the first two stages in the subtractive mode). The two VBG notch filters have identical optical and suppression characteristics differing only in their size: one of them (OptiGrate BNF-532-OD4-11M) is 11 × 11 mm<sup>2</sup>, while the second (OptiGrate BNF-532-OD4-25) is 25 × 25 mm<sup>2</sup>. Each filter provides an optical density of 4 (blocking of >99.99%) at the design wavelength of 532 nm over a bandwidth of <0.3 nm (per manufacturer specifications). It is important that the bandwidth be large enough to block the elastic laser and Rayleigh light but also as narrow as possible in order to preserve most of the spectral extent of the Thomson line shape. The out-of-band light suppression provided by a VBG notch filter is very sensitive to the incidence angle of incoming light, which must be experimentally tuned. High suppression also, therefore, requires that the spread of incidence

angle ( $\Delta\theta$ ) between different rays of light be very small, i.e., the full width at half maximum (FWHM) of angular spread should be  $\lesssim$ 5 mrad. <sup>24</sup> Achieving this small angular spread in spatially resolved setups employing relatively large collection lenses (as benefits absolute signal levels) imposes stringent limits on the optical design as is addressed below.

We have investigated two optical systems for their suitability for spatial imaging and for limiting the spread in incidence angle to the Bragg Notch Filter (BNF): one based on a fiber 7 × 1 linear bundle and the other based on a slit spatial-filter (which has not been previously used in such setups) for improving the sensitivity as needed for temporally resolved measurements. In both cases, the systems serve as an imaging relay between the light collection step (where a 60 mm focal length, 25.4 mm diameter lens collects light from the plasma region) in preparation for approximately collimated incidence on the angle-tuned VBG notch filter (Fig. 1). Both designs seek to (1) gather one-dimensionally spatially resolved LTS light along ~2 mm extent of the beam, (2) preferentially collect light from the region where the LTS is generated vs surrounding regions that contain plasma luminosity only, and (3) prepare the gathered light, with a minimal variation in the beam angle for high suppression by the VBG notch filters. The first configuration focuses the collected light (with a magnification of 0.83 relative to the beam location) into a linear 7 × 1 fiber bundle (Thorlabs BFA105LS02) after which the exit light is collimated and directed to the VBG notch filters. The linear bundle has seven fibers, each with a core diameter of 105  $\mu$ m with the bundle linear axis aligned parallel to the image of the laser beam. The distance between the consecutive fiber centers is 0.13 mm. Light exiting the bundle is collimated with a 40 mm focal length lens and passed to the VBG notch filters yielding a spread in incidence angle of  $\Delta\theta\sim2.5$  mrad (where we approximate  $\Delta\theta\sim$  $d_f/f$ , where  $d_f$  is the fiber diameter and f is the collimating lens focal length). The numerical aperture (NA) of each individual fiber is 0.22; therefore, there is some loss of scattering light due to overfilling of the BNF (light hits the surrounding mask). The second, slit-based, configuration uses two lenses (f = 250 mm and f = 150 mm) confocally surrounding an adjustable linear slit (Thorlabs VA100CP). Similar to the bundle, the axis of the slit is aligned parallel with the image of the laser beam. In this case, the spread in the angle of the light rays to the VBG filters is determined by the combination of the slit width and focal length of the second lens. For the present work, we have  $\Delta\theta \sim 2$  mrad based on a slit width of 300  $\mu$ m, which also yields a magnification of 0.24 relative to the beam location. A 12.7 mm length slit is used, but we reduced the effective length to be 6 mm, since the outer regions of the slit light suffer from reduced attenuation by the VBG filter, which we attribute to the Petzval field curvature (even when an achromatic lens is used). In general, we find that the alignment for the slit spatialfilter configuration is more difficult as compared to the fiber bundle, since it tends to be more difficult to isolate the cause(s) of nonoptimum alignment. The adoption of an f-theta lens, in the future, would be helpful to increase the observation length along the laser beam.

An intensified charge coupled device (ICCD) camera (Princeton Instruments, model PI-MAX4:1024x256-HB-25-P43-S) with a quantum efficiency of 45% at 532 nm was used for the detection of scattered light. The timing was optimized in each optical system with five sets of 2000 accumulated signals (per set) being used to analyze

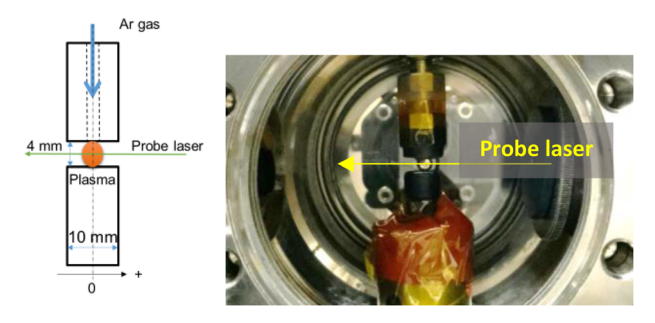


FIG. 2. Schematic and photo of the plasma source. Position along the probe laser is also shown.

the Thomson spectra. The uncertainty in final measured parameters  $(n_e \text{ and } T_e)$  comes from the fitting error and statistical dispersion, so it was evaluated from the uncertainty of the Gaussian (Thomson line shape) fitting and unbiased sample variance. For the conditions of interest, we have incoherent scattering (since the optical wavelength is much less than the Debye length), and so the line shape can be assumed as Gaussian.<sup>27</sup> For the estimation of the electron temperature, we consider instrumental broadening. The calibration of the sensitivity was done by examining signal levels from Rayleigh scattering of argon over a range of pressures (0-40 kPa) and based on the ratio of Thomson and argon Rayleigh scattering cross sections. 28 For LTS measurements, the ICCD gate width is set as 10 ns, considering the jitter of the laser and pulse width as ~8 ns. The exact delay of the ICCD camera gate was optimized for each configuration given small differences in their optical paths (and the fiber refractive index).

Our experiments have employed a custom glow discharge plasma source operating on pure argon as working gas (99.9999% purity), as shown in Fig. 2. Owing to our interest in temporally resolved measurements in connection with oscillations in EP devices, we use a pulsating boost chopper circuit (detail provided in our past work<sup>29</sup>), which works as a harmonic power-supply that has also been demonstrated for external modulation control of Hall thrusters. The voltage between the electrodes is modulated with a fixed frequency of 20 kHz. The source also ignites the plasma at a repetition rate of 20 Hz, which is selected to match the laser pulse-repetition frequency. Figure 3 shows an example of the time history of the discharge current and voltage (averaged over 256 samples). Figure 3(a) is at a zoomed-out time scale and shows the application of high voltage at 20 Hz (period of 50 ms) with the resulting current flow. Figure 3(b) shows a more zoomed-in time scale within the modulation period, showing that the plasma was maintained for about 500 µs (after each ignition) with a peak discharge voltage of about 400 V and a peak current of about 0.3 A. The timing of the Thomson probe laser relative to the discharge modulation is controlled with a delay-generator supplying signals to the laser.

#### **III. RESULTS**

Figure 4 shows an example of spectral attenuation data for cases of one and two VBG notch filters recorded in this case with

-100 0 100 200 300

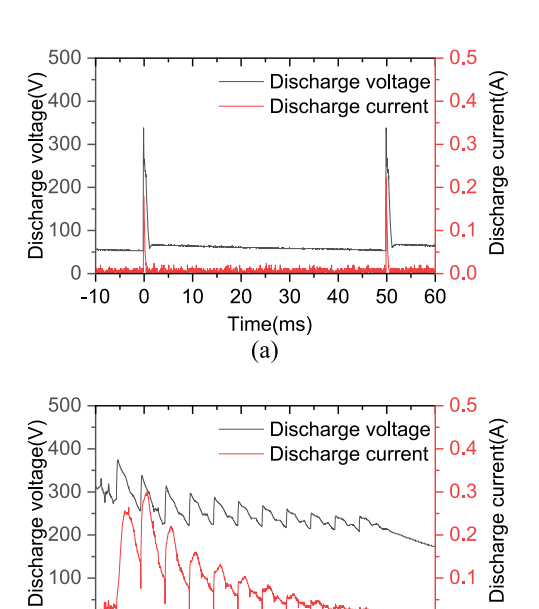


**FIG. 3.** Time history of the discharge current and discharge voltage between two electrodes as viewed over (a) a long time-duration (from -10 to +60 ms) and (b) a short time-duration (from -100 to +600  $\mu$ s).

Time(µs)

(b)

400 500 600

the fiber bundle setup. Here, the attenuation is defined as the ratio of the signal at the given wavelength with the filter(s) to the peak signal at the laser wavelength including Rayleigh scattering without the filter(s) recorded for 40 kPa argon gas. With inadequate filter suppression, one would have an appreciable signal (due to Rayleigh and/or background scatter) at the laser line-center wavelength (~532 nm), which can then preclude the measurement of LTS spectra. In our case, at the line-center, we find the attenuation of optical density of ~4 with one filter and optical density of ~5 or more with two filters, showing that a strong suppression is achieved. The suppression derived from using two filters is essential for the temporally resolved measurement. At wavelengths far from the line center, the attenuation (as defined here) is high simply due to being away from the Rayleigh wavelength (also confirming that the detector is not spilling light into adjacent wavelength bins). The high attenuation across the spectrum is important for low plasma number density measurements (conditions with  $n_e \lesssim 10^{17} \text{ m}^{-3}$ ). In the case with two BNFs, no discernible signal can be observed across the spectrum in the absence of LTS light. (Note that the negative values of attenuation are numeric artifacts due to negligible signals being sometimes recorded as negative numbers after the background subtraction step.)

Figure 5 shows the spatial dependence of the signal sensitivity recorded for both the bundled fiber and slit spatial-filter configurations. Here, the sensitivity (detection system response) is estimated from the Rayleigh scattering signal based on the slope of the argon Rayleigh signal vs pressure (in arbitrary units), as shown in Fig. 6.

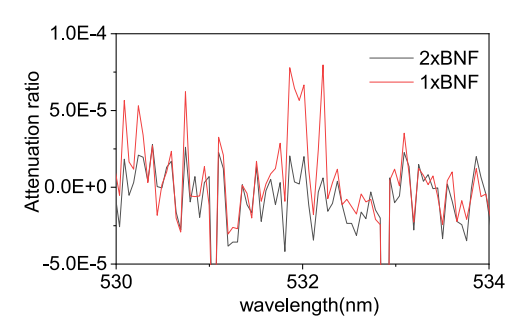


**FIG. 4.** Attenuation ratio of the signal as a function of wavelength (referenced to 40 kPa argon Rayleigh scattering as measured at the line center).

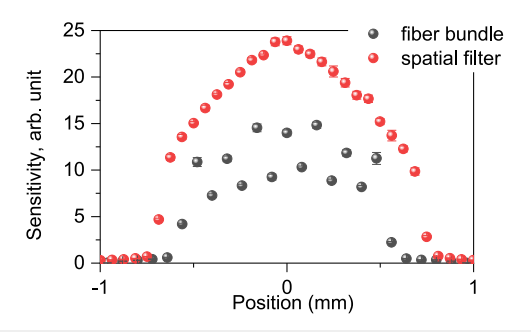


**FIG. 5.** Spatial distribution of the sensitivity for two systems found from Rayleigh scattering of argon. The abscissa axis shows the position along the probe laser with the origin corresponding to the center of the electrodes (see Fig. 2). The position increases in the laser propagation direction.

The spatial position axis corresponds to the observation position along the probe laser path. The parameters of the fiber and slit are as given above. The sensitivity profile recorded with the fiber bundle shows a spatially varying structure, which is due to the light passing through the seven individual fibers comprising the bundle. Note that due to the selected CCD binning and magnification, there is not a direct correspondence between the images from the fibers and pixels (and we did not want to limit to only seven pixels); however, one can see seven elevated pixels corresponding to the individual fibers. The profile for the slit case is more uniform with a fall-off on the edges due mostly to the Petzval field curvature. The better sensitivity with the spatial-filter, by a factor of ~2, is primarily due to the coupling losses of the fiber bundle. The achievable spatial resolution of the setup is determined by the pixel size of the ICCD camera  $(26 \,\mu\text{m})$  and the binning, where, for the wavelength axis, we bin two pixels together and, for the spatial axis, we bin four pixels together. The spatial resolution difference between the bundle fiber and the spatial-filter is due to the difference in lens magnification for the two

Figure 7 shows the example raw spectra for the two configurations (fiber bundle and slit spatial-filter) recorded at a time of 12.5  $\mu$ s relative to the modulation origin (i.e., 1/4 of the way through the fast modulation period) and spatial position of zero (i.e., at the center position of light collection along the beam) for three conditions:

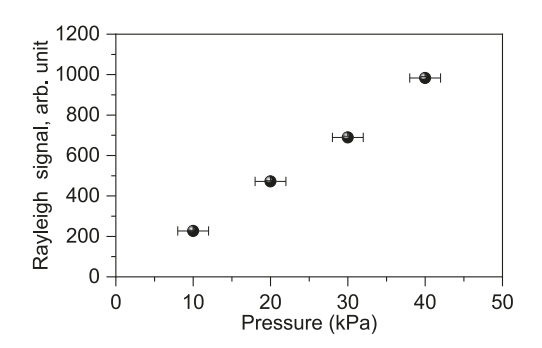
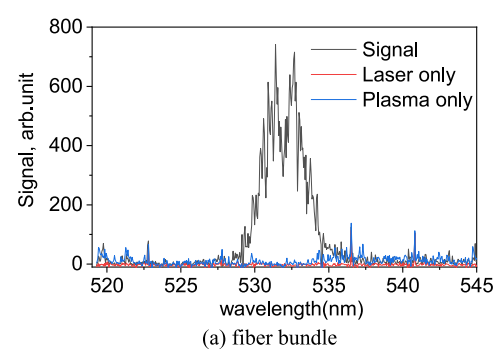
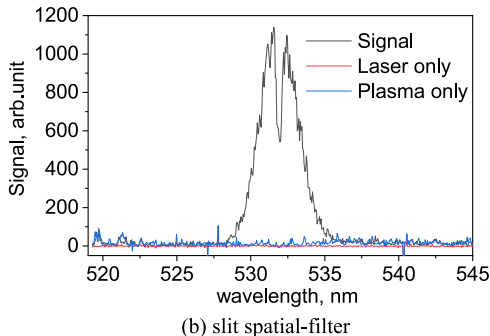


FIG. 6. Argon Rayleigh signal vs pressure at the origin position.





**FIG. 7.** Spectra for two systems at  $t = 12.5 \mu s$  and the position of 0 mm from the (a) bundled fiber system and (b) slit spatial-filter system.

plasma with laser (labeled signal), laser without plasma (labeled laser only), and plasma without laser (labeled plasma only). The argon mass flow rate was kept constant for each of the three cases. There is little difference between the two Thomson spectra (curves labeled signal). In both cases, no stray light can be observed (i.e., no Rayleigh or background peak at the line center) and weak emission lines are detected around 520 and 542 nm. Figure 7 also shows that the noise with a fiber bundle is relatively larger than that with a spatial-filter due to the difference in the sensitivity (Fig. 5). The center dip is due to the BNF profiles and due to the instrument function of the spectrometer, so the signal does not fully reduce to zero at the laser wavelength.

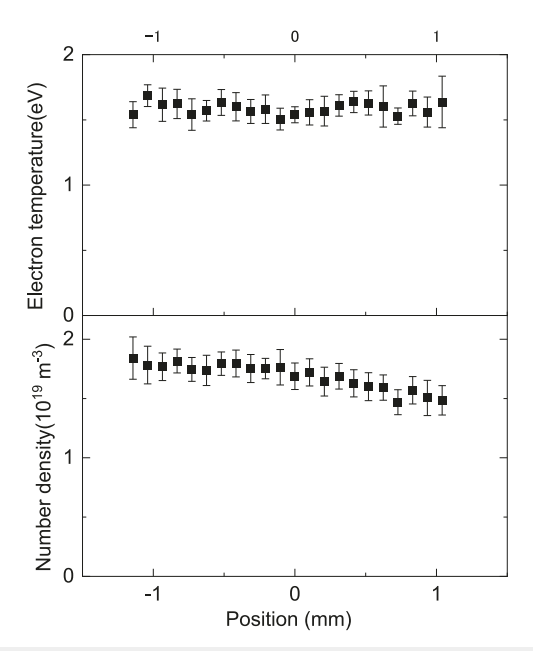


**FIG. 8.** Spatial distribution of the plasma property along the probe laser at  $t=12.5~\mu \mathrm{s}$ .

Figure 8 shows the spatial distribution of plasma properties along the probe laser recorded again at a quarter period after t = 0(i.e.,  $t = 12.5 \mu s$ ). The inferred plasma properties are found from data like Fig. 7 where the LTS signal was obtained by subtracting the signals of laser only and plasma only from the signals with laser and plasma. The resulting spectra are fit with a Gaussian function (Thomson line shape) with an excluded region around the laser wavelength ( $\pm 0.5$  nm). Instrumental broadening is accounted for in the fitting but has a negligible impact on the fitting (given that the instrument function width of 0.15 nm is significantly narrower than the measured LTS spectral widths). The data analysis has also corrected for the spatial dependence of sensitivity (Fig. 5). The resulting electron temperature is fairly uniform (within uncertainty) along the recorded extent, while the number density seems to show a reduction toward the positive side, likely due to the detailed electrode shape and position (which were nominally symmetric across the measurement region but with some shape and alignment complexity at the sub-mm scale). The uncertainty of the electron temperature at the origin position is 0.06 eV due to the fitting error and a variation in the width of the Thomson scattering spectra, and the averaged electron temperature is 1.54 eV, giving a fractional uncertainty of 0.04. The average fractional uncertainty varies with position and is 0.065 across the 22 measured points. The uncertainty of number density at the origin is  $1 \times 10^{18}$  m<sup>-3</sup> due to the relatively large variation in signal intensity (plasma density fluctuations), and the average number density is  $1.7 \times 10^{19}$  m<sup>-3</sup>, giving a fractional uncertainty of 0.06. In this case, the average fractional uncertainty of all 22 points is 0.10. For both electron temperature and density, the uncertainties near the edge of the slit are somewhat higher

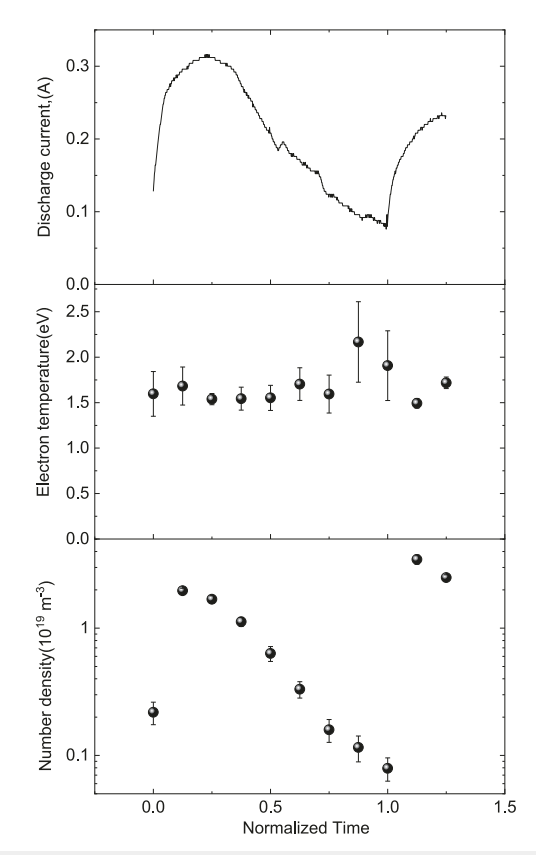


**FIG. 9.** Time histories of the plasma parameters vs normalized time, where the time is normalized by the switching period of 50  $\mu$ s.

 $[n_e = (15 \pm 1.2) \times 10^{18} \text{ m}^{-3}, T_e = (1.6 \pm 0.2) \text{ eV}]$  than in the center owing to weaker light signals.

Figure 9 shows the time history of the plasma properties at the spatial position of zero for the modulated plasma along with the discharge current trace (averaged for 256 waveforms). Here, the time is normalized by the period of the discharge voltage, i.e., by 50  $\mu$ s. The number density shows very similar trends as the discharge current increases from T = 0 to  $T \sim 0.125$ , then gradually decreases until  $T \sim 1$ , and then exhibits a notable upward jump at  $T \sim 1.125$ . (Note that given the ringing nature of the discharge, each subsequent 50  $\mu$ s period behaves differently from the previously discussed ones, so we do not expect to have the same parameter values at T = 1.125as T = 0.125—see the top of Figs. 3 and 7.) The number density at T = 1 is  $n_e = (7.9 \pm 1.6) \times 10^{17}$  m<sup>-3</sup>, which is almost the same number density as one encounters at typical Hall thruster conditions, as we are interested in. The relatively large uncertainty in  $n_e$ of ~±20%, under this condition, is primarily due to the weak signal level and can be improved by increasing the number of signal accumulations (measurement time) or by the use of larger optics to collect the scattering signal. Meanwhile, the electron temperature is almost constant at  $T_e \sim 1.6$  eV, though somewhat elevated at  $T \sim 1$ .

#### IV. SUMMARY

For the first time, a portable temporally resolved Thomson scattering measurement system has been developed and used to measure temporally varying plasma parameters (electron temperature and electron number density) in a low-density discharge. We have divided the fast modulation period of 50  $\mu s$  into eight temporal steps and can resolve plasma dynamics on that time scale. The oscillation period studied was selected to be representative of fluctuations in EP Hall-effect thrusters. Future studies in thruster devices can be performed by synchronizing the detection with natural oscillations or by deliberately modulating the anode current (with a power supply similar to that used here) as has been previously demonstrated. 19 Spatial resolution at the sub-mm level has also been demonstrated. Attaining simultaneous spatial- and temporalresolution in low density plasmas places stringent requirements on the S:N and suppression of the measurement system. We find an optimum setup based on the use of two VBG notch filters to suppress the Rayleigh scattering signal and stray light from walls, which is an important requirement to enable low density plasma measurements. In summary, we have shown spatially and temporally resolved measurements of a low density plasma using a compact and potable LTS measurement system. This system can contribute toward revealing the unrevealed physics in Hall thruster, such as anomalous transport or neutralization mechanism in Hall thrusters. The diagnostic system can also be used for other temporally varying low density plasmas of practical interest, for example those used for semiconductor processing.

#### **ACKNOWLEDGMENTS**

This work was supported by JSPS KAKENHI under Grant Nos. JP18H03815, JP18KK0406, and JP22H00243. This work was also supported by the National Science Foundation Division of Physics under Award No. 2010466. Comments and suggestions from Mr. Jacob Gottfried were greatly appreciated.

# **AUTHOR DECLARATIONS**

# **Conflict of Interest**

The authors have no conflicts to disclose.

# **Author Contributions**

Naoji Yamamoto: Conceptualization (equal); Formal analysis (lead); Investigation (lead); Methodology (equal); Writing – original draft (lead); Writing – review & editing (supporting). Azer Yalin: Conceptualization (equal); Formal analysis (supporting); Investigation (supporting); Methodology (supporting); Resources (lead); Writing – original draft (supporting); Writing – review & editing (lead).

### **DATA AVAILABILITY**

The data that support the findings of this study are available from the corresponding author upon reasonable request.

#### **REFERENCES**

- <sup>1</sup>J. Sheffield, *Plasma Scattering of Electromagnetic Radiation* (Academic Press, New York, 1975), Chap. 9.
- <sup>2</sup>D. E. Evans and J. Katzenstein, Rep. Prog. Phys. **32**(1), 207–271 (1969).
- <sup>3</sup>K. Muraoka, K. Uchino, and M. D. Bowden, Plasma Phys. Controlled Fusion 40(7), 1221–1239 (1998).
- <sup>4</sup>K. Tomita, N. Yamamoto, N. Yamasaki, T. Tsuru, K. Uchino, and H. Nakashmia, J. Propul. Power **26**(2), 381–383 (2010).
- <sup>5</sup>S. Tsikata, C. Honoré, and D. Grésillon, J. Instrum. **8**, C10012 (2013).
- <sup>6</sup>B. Vincent, S. Tsikata, and S. Mazouffre, Plasma Sources Sci. Technol. 29(3), 035015 (2020).
- <sup>7</sup>K. Kouge, K. Tomita, J. Hotta, Y. Pan, H. Tomuro, T. Yanagida, K. Uchino, and N. Yamamoto, Jpn. J. Appl. Phys. **61**(5), 056001 (2022).
- <sup>8</sup>Y. Pan, K. Tomita, Y. Kawai, M. Matsukuma, and K. Uchino, Jpn. J. Appl. Phys. **60**, SAAB03 (2021).
- <sup>9</sup>N. Yamamoto, K. Tomita, K. Sugita, T. Kurita, H. Nakashima, and K. Uchino, Rev. Sci. Instrum. **83**, 073106 (2012).
- <sup>10</sup> K. Tomita, Y. Sato, S. Tsukiyama, T. Eguchi, K. Uchino, K. Kouge, H. Tomuro, T. Yanagida, Y. Wada, M. Kunishima, G. Soumagne, T. Kodama, H. Mizoguchi, A. Sunahara, and K. Nishihara, Sci. Rep. 7, 12328 (2017).
- 11 J. M. Fife, M. Martinez-Sanchez, and J. Szabo, AIAA Paper No. 97-3052, 1997.
- <sup>12</sup>J. P. Boeuf and L. Garrigues, J. Appl. Phys. **84**, 3541–3554 (1998).
- <sup>13</sup>K. Hara and *et al.*, "Perturbation analysis of ionization oscillations in Hall effect thrusters," Phys. Plasmas **21**(12), 122103 (2014).
- <sup>14</sup>O. Chapurin and *et al.*, "On the mechanism of ionization oscillations in Hall thrusters," J. Appl. Phys. **129**(23), 233307 (2021).
- <sup>15</sup>Y. Esipchuck and *et al.*, "Plasma oscillations in closed-drift accelerators with an extended acceleration zone," Sov. Phys. Tech. Phys. 18, 928 (1974).
- <sup>16</sup> N. Yamamoto, K. Komurasaki, and Y. Arakawa, J. Propul. Power 21(5), 870–876 (2005).

- <sup>17</sup>M. J. Sekerak and *et al.*, "Mode transitions in Hall-effect thrusters induced by variable magnetic field strength," J. Propul. Power **32**(4), 903–917 (2016).
- <sup>18</sup>B. A. Jorns and R. R. Hofer, "Plasma oscillations in a 6-kW magnetically shielded Hall thruster," Phys. Plasmas 21, 053512 (2014).
- <sup>19</sup>R. B. Lobbia, "A time-resolved investigation of the Hall thruster breathing mode," Ph.D. thesis (University of Michigan, MI, 2010), p. 179, https://pepl.engin.umich.edu/pdf/2010\_Lobbia\_Thesis.pdf.
- <sup>20</sup>V. H. Chaplin and *et al.*, "Time-resolved ion velocity measurements in a high-power Hall thruster using laser-induced fluorescence with transfer function averaging," Appl. Phys. Lett. **116**(23), 234107 (2020).
- <sup>21</sup>N. Kuwabara and *et al.*, "Electron density measurement inside a Hall thruster using microwave interferometry," J. Propul. Power 37(3), 491–494 (2021).
- <sup>22</sup>B. A. Jorns and *et al.*, "Prediction and mitigation of the mode transition in a magnetically shielded Hall thruster at high-specific impulse and low power," in 37th International Electric Propulsion Conference, Cambridge, MA, 2022.
- <sup>23</sup> J. A. Gottfried and *et al.*, "Collective Thomson scattering measurement of plasma evolution during the current pulse in a laser-triggered switch," Appl. Phys. Lett. 121, 244101 (2022).
- <sup>24</sup>B. Vincent, S. Tsikata, S. Mazouffre, T. Minea, and J. Fils, Plasma Sources Sci. Technol. 27(5), 055002 (2018).
- <sup>25</sup> J. Bak, J. L. Suazo Betancourt, A. Rekhy, A. Abbasszadehrad, R. B. Miles, C. M. Limbach, and M. L. R. Walker, Rev. Sci. Instrum. 94, 023003 (2023).
- <sup>26</sup> A. J. Friss and A. P. Yalin, Opt. Lett. **43**(21), 5343–5346 (2018).
- <sup>27</sup>I. H. Hutchinson, *Principles of Plasma Diagnostics* (Cambridge University Press, 2005).
- <sup>28</sup> A. W. DeSilva and G. C. Goldenbaum, in *Plasma Physics: Part A (Methods of Experimental Physics)*, edited by R. H. Lovberg and H. R. Griem (Academic Press, New York, 1971), Chap. 3, Vol. 9.
- <sup>29</sup> N. Yamamoto, H. Takegahara, J. Aoyagi, K. Kuriki, T. Tamida, and H. Osuga, IEEE Trans. Plasma Sci. 43(1), 158–164 (2015).